CD GALAXY CONTRIBUTION TO THE STRONG LENSING CROSS SECTIONS OF GALAXY CLUSTERS

MASSIMO MENEGHETTI[1,2], MATTHIAS BARTELMANN[2], LAURO MOSCARDINI[1]
[1]DIPARTIMENTO DI ASTRONOMIA, UNIVERSITÀ DI PADOVA, VICOLO DELL'OSSERVATORIO 2, I–35122 PADOVA, ITALY
[2]MAX-PLANCK-INSTITUT FÜR ASTROPHYSIK, KARL-SCHWARZSCHILD-STRASSE 1, D–85748 GARCHING, GERMANY

MNRAS, submitted

ABSTRACT

We perform ray-tracing simulations evaluating the effect of a cD galaxy on the strong lensing properties of five galaxy cluster halos obtained from N-body simulations. The cD galaxy is modelled using both axially symmetric and elliptical models and assuming several masses for its dark matter halo. The effect of the cD orientation with respect to the mass distribution of the host galaxy cluster is also investigated. The simulations are carried out in an open and a flat model universe with cosmological constant. We find that the enhancement of the cluster lensing cross sections for long and thin arcs due to the presence of a massive cD at the cluster centre is typically less than 100%, depending on the model used for the cD galaxy and its orientation. The impact of the cD on the cluster efficiency for producing radially magnified images is larger only for those clusters whose lensing cross section for radial arcs is very small in absence of the central galaxy. We conclude that the presence of a cD galaxy at the cluster centre can only moderately influence the cluster efficiency for strong lensing and in particular fails to explain the discrepancy between the observed number of giant arcs in galaxy clusters and their abundance predicted from lensing simulations in the currently most favoured ΛCDM model.

1. INTRODUCTION

Many authors have pointed out that the observed abundance of gravitational arcs whose length-to-width ratio exceeds a given threshold can be used for constraining the cosmological model and its parameters. Indeed, the occurrence of those rare events caused by highly non-linear effects in cluster cores is determined by several factors related to the geometry of the universe, as well as to the abundance, evolution and internal structure of the lensing clusters, which all depend on cosmology.

Investigating the lensing properties of a large sample of numerically modelled galaxy clusters using the ray-tracing technique, Bartelmann et al. (1998) showed that the expected number of *giant* arcs, usually defined as arcs with length-to-width ratio exceeding 10 and apparent *B*-magnitude less than 22.5 (Wu & Hammer 1993), changes by orders of magnitude between different cosmological models. In particular, they found that the expected number of giant arcs is smaller by a factor of ten in a flat, low density universe with a matter density parameter $\Omega_0 = 0.3$ and a cosmological constant $\Omega_\Lambda = 0.7$ (ΛCDM) than in an open, low-density cosmological model with $\Omega_0 = 0.3$ and $\Omega_\Lambda = 0$ (OCDM).

Observations of the abundance of gravitational arcs in galaxy clusters seem to be consistent only with the predictions for an open universe (Bartelmann et al. 1998; Le Fevre et al. 1994; Gioia & Luppino 1994). This is in pronounced disagreement with other observational results, in particular those obtained from the recent experiments on the cosmic microwave background (de Bernardis et al. 2002) and the observations of high-redshift type-Ia supernovae (Perlmutter et al. 1997; Perlmutter 1998), which all suggest instead that the cosmological model most favoured by the data is spatially flat and dominated by a cosmological constant.

Several studies tried to resolve this inconsistency, but satisfactory explanations remain to be found. Similar estimates of the number of long and thin arcs were attempted adopting isothermal analytic instead of numerical cluster lens models (Cooray, Quashnock & Miller 1999; Kaufmann & Straumann 2000). The results of these studies differ from those of Bartelmann et al. (1998) in that they are almost insensitive to the cosmological constant and predict similar abundances of arcs in the ΛCDM and in the OCDM models. However, Meneghetti, Bartelmann & Moscardini (2002) recently showed that analytic models are inadequate for quantitative studies of arc statistics, because asymmetries and substructures in the deflector play a relevant role for determining the galaxy cluster efficiency for strong lensing and cannot properly be taken into account when using simple analytic models for modelling cluster lenses. Moreover, Bartelmann et al. (2003) demonstrated that elliptical cluster models with the density profile found in numerical simulations by Navarro et al. (1996) were able to reproduce the relative change of an order of magnitude in the arc cross sections produced by clusters in the ΛCDM and OCDM models.

Meneghetti et al. (2001) also investigated the effect of cluster galaxies on arc statistics but found that they do not introduce perturbations strong enough for significantly changing the number of arcs and the distributions of lengths, widths, curvature radii and length-to-width ratios of long arcs.

However, the possible effects due to the presence of a massive cD galaxy near the cluster centre were not investigated there. The centres of massive galaxy clusters are generally dominated by such very massive ($\sim 10^{13} M_\odot$) galaxies, which could in principle noticeably affect the strong-lensing properties of their host clusters. In fact, due to their more concentrated dark matter halos, they may steepen the inner slope of the cluster density profile and push the cluster critical curves to larger distances from the centre. Thus, the length of the critical curves may be increased, and thus the probability for long arcs to form. Moreover, cD galaxies may help their host clusters to reach the critical central surface density for producing critical curves and becoming efficient strong lenses.

Understanding the effect of massive central galaxies on the strong lensing properties of galaxy clusters is an important issue also because several studies attempted using arc statistics for constraining the density profiles of lenses or the nature of the dark matter composing their halos (Wu & Mao 1996; Molikawa et al. 1999; Oguri et al. 2001; Molikawa & Hattori 2001; Oguri et al. 2002; Meneghetti et al. 2001). The conclusions from all these studies may change should the effect of a central massive galaxy turn out to be relevant.

Thus, we investigate in this paper whether the presence of a massive cD galaxy at the centre of a galaxy cluster can significantly change the cluster's ability to produce strong lensing events and reconcile the lensing cross section of ΛCDM clusters with the observations. For doing so, we study the lensing properties of a sample of five galaxy clusters numerically simulated in both the ΛCDM and the OCDM cosmological models, and we measure their efficiency for producing tangential and radial arcs before and after the inclusion of a cD galaxy. The central galaxy is modelled using both axially symmetric and elliptical models and assuming a range of virial masses and possible orientations with respect to the mass distribution of the host cluster.

The plan of the paper is as follows. In Section 2., we use simple analytic models for qualitatively estimating the impact of a cD galaxy on the strong lensing properties of galaxy clusters. In Section 3., we describe the numerical models used and the methods adopted for the lensing simulations. The results are discussed in Section 4.. Finally, conclusions are summarised in Section 5..

2. EXPECTATIONS

We begin by investigating with the help of analytical models what impact we can expect from cD galaxies on the strong-lensing properties of galaxy clusters. We will use two different analytic lens models, one with a singular isothermal density profile, and the other with the density profile found in numerical simulations by Navarro et al. (1996; hereafter NFW).

2.1. *Axially symmetric models*

The radial density profile of a singular isothermal sphere (hereafter SIS) is given by

$$\rho(r) = \frac{\sigma_v^2}{2\pi G r^2} \,, \tag{1}$$

where σ_v is the velocity dispersion of the halo. The NFW density profile is instead given by

$$\rho(r) = \frac{\rho_s}{(r/r_s)(1+r/r_s)^2} \,, \tag{2}$$

where ρ_s and r_s are characteristic density and distance scales, respectively (see Navarro et al. 1997). These two parameters are not independent. The ratio between r_s and the radius r_{200} within which the mean halo density is 200 times the critical density is called concentration, $c = r_{200}/r_s$. As results from numerical simulations show, the concentration parameter c can be expressed as a function of the halo virial mass, which thus is the only free parameter. The concentration also depends on the cosmological model, implying that the lensing properties of haloes with identical mass are different in different cosmological models if they are modelled as NFW spheres. The NFW halo profile falls off steeper than isothermal at radii beyond r_s, but flattens towards the halo centre. These different features lead to markedly different lensing properties of the NFW compared to the SIS model (see the discussions in Perrotta et al. 2002 and Meneghetti et al. 2003).

Several algorithms were developped for computing the concentration parameter from the halo virial mass (Navarro et al. 1997; Bullock et al. 2001; Eke et al. 2001). They are all based on the findings that numerically simulated haloes tend to be more concentrated the earlier they form, and that their central density reflects the mean cosmic density at their formation time. Since haloes of lower mass form earlier in hierarchical models than haloes of higher mass, the concentration is a decreasing function of the halo mass.

In this work, we adopt the algorithm proposed by Navarro et al. (1997), which first assigns to a halo of mass M a collapse redshift $z_{\rm coll}$ defined as the redshift at which half of the final mass is contained in progenitors more massive than a fraction f of the final mass. Then the density scale of the halo is assumed to be some factor C times the mean cosmic density at the collapse redshift. They recommend setting $f = 0.01$ and $C = 3 \times 10^3$ because their numerically determined halo concentrations were well fit adopting these values.

In the case of axially symmetric models the computation of the deflection angles reduces to a one-dimensional problem. We define the optical axis as the straight line passing through the observer and the lens centre and introduce the physical distances perpendicular to the optical axis on the source and lens planes, ξ and η, respectively. We then fix a length scale ξ_0 on the lens plane and define the dimensionless distance $x \equiv \xi/\xi_0$ from the lens centre. By projecting ξ_0 on the source plane, we define a corresponding length scale $\eta_0 = \xi_0 (D_s/D_l)$ on the source plane, where D_s and D_l are the angular diameter distances to the source and lens planes, respectively. Like on the lens plane, we define a dimensionless distance from the optical axis $y \equiv \eta/\eta_0$ on the source plane.

Using this dimensionless formalism, the lensing potential of a SIS lens can be written as

$$\psi(x) = |x| \,, \tag{3}$$

if $\xi_0 = 4\pi(\sigma_v/c)^2 (D_l D_{ls}/D_s)$ is chosen as a length scale, where D_{ls} is the angular-diameter distance between lens and source. The derivative of the lensing potential with respect to x is the reduced deflection angle at distance x,

$$\alpha(x) = \frac{x}{|x|} \,. \tag{4}$$

For an NFW sphere, we choose $\xi_0 = r_s$ and define $\kappa_s \equiv \rho_s r_s \Sigma_{\rm cr}^{-1}$, where $\Sigma_{\rm cr} = [c^2/(4\pi G)]\,[D_s/(D_l D_{ls})]$ is the critical surface mass density for strong lensing. Its lensing potential then reads

$$\Psi(x) = 4\kappa_s g(x) \,, \tag{5}$$

where

$$g(x) = \frac{1}{2}\ln^2\frac{x}{2} + \begin{cases} 2\arctan^2\sqrt{\frac{x-1}{x+1}} & (x>1) \\ -2\,\mathrm{arctanh}^2\sqrt{\frac{1-x}{1+x}} & (x<1) \\ 0 & (x=1) \end{cases} \,. \tag{6}$$

This implies the deflection angle

$$\alpha(x) = \frac{4\kappa_s}{x} h(x) \,, \tag{7}$$

with

$$h(x) = \ln\frac{x}{2} + \begin{cases} \frac{2}{\sqrt{x^2-1}}\arctan\sqrt{\frac{x-1}{x+1}} & (x>1) \\ \frac{2}{\sqrt{1-x^2}}\,\mathrm{arctanh}\sqrt{\frac{1-x}{1+x}} & (x<1) \\ 1 & (x=1) \end{cases} \,. \tag{8}$$

(Meneghetti et al. 2003; Bartelmann 1996).

2.2. *Elliptical model*

Lensing by galaxy clusters can only crudely be described by axially symmetric models because their generally high level of asymmetry and substructure changes their lensing properties qualitatively and substantially. We thus perturb the axially symmetric lens models such that their lensing potentials (3)) and (5) acquire elliptical isocontours. We define the ellipticity as $e \equiv 1 - b/a$, where a and b are the major and minor axes of the ellipse, respectively, and introduce it into (5) by substituting

$$x \to \mathcal{X} = \sqrt{\frac{x_1^2}{(1-e)} + x_2^2(1-e)}\,, \tag{9}$$

where x_1 and x_2 are the two Cartesian components of x, $x^2 = x_1^2 + x_2^2$. The Cartesian components of the new deflection angle are

$$\begin{aligned} \alpha_1 &= \frac{\partial\psi}{\partial x_1} = \frac{x_1}{(1-e)\mathcal{X}}\hat{\alpha}(\mathcal{X})\,, \\ \alpha_2 &= \frac{\partial\psi}{\partial x_2} = \frac{x_2(1-e)}{\mathcal{X}}\hat{\alpha}(\mathcal{X})\,, \end{aligned} \tag{10}$$

where $\hat{\alpha}(\mathcal{X})$ is the unperturbed (i.e. axially-symmetric) deflection angle at the distance $\mathcal{X}$ from the lens centre.

2.3. *Estimates*

Arcs form close to the tangential critical curve of a lens from sources close to the tangential caustic. For axially symmetric lens models, the tangential critical curve encloses a circle which encloses an average convergence of unity, so that

$$\frac{2}{\theta_t^2}\int_0^{\theta_t} \kappa(\theta')\,\theta'\mathrm{d}\theta' = 1 \tag{11}$$

defines the radius θ_t of the tangential critical curve. For singular isothermal spheres,

$$\theta_t = 4\pi\left(\frac{\sigma_v}{c}\right)^2 \frac{D_{ls}}{D_s}\,, \tag{12}$$

which is approximately proportional to the lens mass. A similar closed expression cannot be given for an NFW sphere. The tangential critical radius of a set of concentrically superposed SIS lens models is simply the sum of the tangential critical radii of the individual components. This implies that adding a cD galaxy of $\sim 10^{13}h^{-1}M_\odot$ extends the tangential critical curve of a cluster of $\sim 5\times10^{14}h^{-1}M_\odot$ by a few per cent only.

However, the situation changes remarkably if the cD galaxy, modelled as a SIS, is added to a cluster with an NFW density profile. The comparatively flatter density profile near the cluster centre causes the cD galaxy to have a much stronger effect, as Fig. 1 illustrates.

The two curves shown in the figure are the ratios between the tangential critical radii of a cluster with virial mass $7.5\times10^{14}h^{-1}M_\odot$ with and without a cD galaxy of virial mass $10^{13}h^{-1}M_\odot$ added to its centre. The solid and dotted curves are obtained for clusters with SIS and NFW density profiles, respectively. The curves show how these ratios change with the ellipticity e of the cluster's lensing potential. The tangential critical curves are circles only for $e = 0$; for $e > 0$, we use their maximum cluster-centric distance instead.

Two results can be read off Fig. 1. First, the effect of a cD galaxy of fixed mass on the tangential critical curves of a cluster of fixed mass is much more pronounced if the cluster has an NFW rather than a SIS density profile; and second, the effect of the cD decreases as the ellipticity of the cluster increases because the increased shear of the cluster makes the additional surface mass density relatively less important. For the axially symmetric NFW cluster, the cD extends the tangential critical curve by as much as 38%, although it has only a few per cent of the cluster's mass! Numerical simulations suggest ellipticities of ~ 0.3, for which the effect drops $\sim 12\%$.

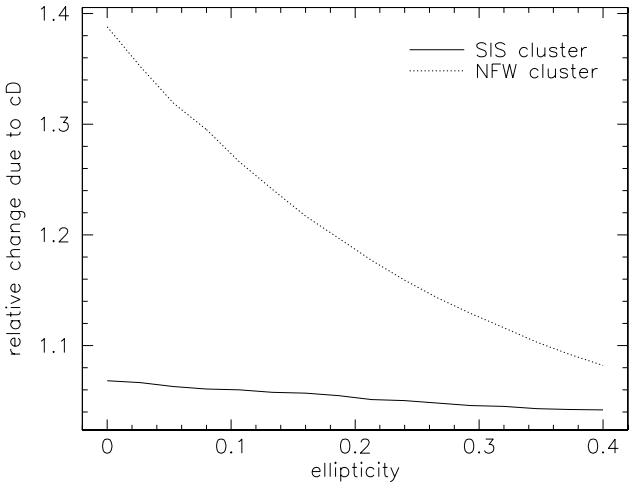

FIG. 1.—The two curves show the ratios between the tangential critical radii of a cluster of virial mass $7.5\times10^{14}h^{-1}M_\odot$ with and without a cD galaxy of virial mass $10^{13}h^{-1}M_\odot$ added to its centre. The solid and dotted curves were obtained modelling the cluster with a SIS or NFW density profile, respectively. The ratios are given as functions of the ellipticity e of the cluster potential, as described in the text. Since tangential critical curves are not circular for $e > 0$, we use their maximum cluster-centric distance instead.

Since we have good reasons to believe that clusters are better described by NFW than by SIS density profiles, the figure illustrates that an estimate of the effect of cD galaxies on strong lensing by clusters based on SIS models alone can be highly misleading. In addition, the change with cluster ellipticity is important because it shows that the enhanced gravitational shear due to asymmetries and substructure in the cluster potential reduces the impact of the cD galaxy.

It is a second interesting question whether the impact of a cD galaxy on a cluster lens changes with cluster redshift. Again, for two concentrically superposed SIS lenses, the relative change in the tangential critical radii is exactly independent of redshift, but this does not need to hold true for cluster lenses with NFW density profile. We show in Fig. 2 as a function of lens redshift the maximum extent of the tangential critical curve and the corresponding caustic for a cluster with NFW density profile and virial mass $7.5\times10^{14}h^{-1}M_\odot$, with and without a cD galaxy with singular isothermal density profile and virial mass $10^{13}h^{-1}M_\odot$. The cluster's lensing potential is assumed to have ellipticity $e = 0.3$, in good agreement with values found in numerical simulations.

The curves end where the maximum extent of the tangential critical curve drops below $10''$, because arcs formed near smaller tangential critical curves can hardly be classified as large arcs. The curves illustrate that the relative change in the dimensions of tangential critical curves and caustics is remarkably insensitive to the lens redshift, even if the cluster is assumed to have an NFW density profile.

We now turn to numerical cluster models in order to test the impact of cD galaxies on cluster lensing with more realistic clus-

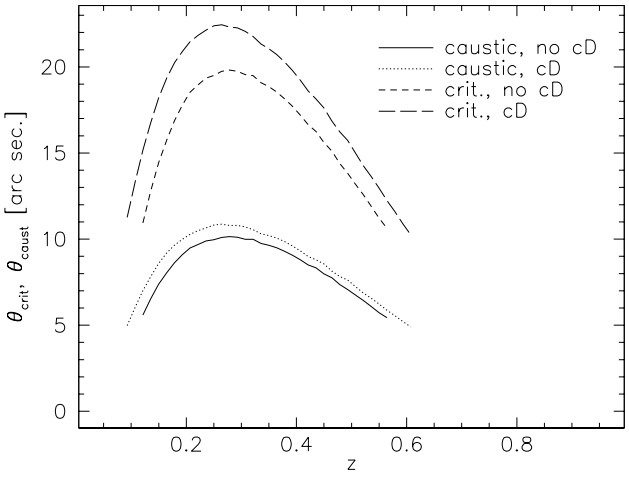

FIG. 2.—The curves show, as functions of lens redshift, the maximum extent of tangential critical curves and corresponding caustics of a cluster with NFW density profile and virial mass $7.5\times10^{14}\,h^{-1}\,M_\odot$, with and without a cD galaxy with singular isothermal density profile and virial mass $10^{13}\,h^{-1}\,M_\odot$. An ellipticity of $e=0.3$ was assumed for the cluster's lensing potential, and the source redshift is $z_s=1$. Obviously, the impact of a cD galaxy is highly insensitive to the lens redshift. The curves end where the maximum extent of the tangential critical curves drops below $10''$ because we are interested in the formation of large arcs only, which require a minimum size of the tangential critical curves.

ter mass distributions.

3. NUMERICAL MODELS

3.1. Simulated Clusters

We investigate the lensing properties of a sample of five numerically simulated cluster-sized dark matter halos kindly made available by the GIF collaboration (Kauffmann et al. 1999). The same clusters were used by Bartelmann et al. (1998). They were obtained from N-body simulations performed in the framework of several cosmological models. In this paper, we only use the simulations for a flat model with cosmological constant (ΛCDM), which has $\Omega_0=0.3$, $\Omega_\Lambda=0.7$ and $h=0.7$, and in an open model without cosmological constant (OCDM, $\Omega_0=0.3$, $h=0.7$).

The initial matter density in these models is perturbed about the mean according to a CDM power spectrum (Bond & Efstathiou 1984) with primordial spectral index $n=1$, normalised such that the local abundance of massive galaxy clusters is reproduced (e.g. Viana & Liddle 1996). The complete list of cosmological parameters in these simulations is given in Bartelmann et al. (1998).

For each cosmological model, an initial simulation with $N=256^3$ particles in a box of $141\,h^{-1}$Mpc side length was run. The mass of individual particles is $1.4\times10^{10}h^{-1}M_\odot$. Clusters were obtained from initial cosmological simulations as follows. High density regions were identified by means of a standard friends-of-friends algorithm, selecting only the dense cores of the collapsed objects. Around the centres of those, all particles were collected which lie within a sphere of radius $1.5\,h^{-1}$Mpc, corresponding to the Abell radius. These objects are taken as clusters. For our analysis, we took the five most massive clusters in the simulation volumes.

As shown by Bartelmann et al. (1998), the maximum efficiency for the production of long and thin arcs is reached by these clusters when their redshift is in the range $0.2\lesssim z\lesssim0.4$. Since our analytic estimates showed that the lens redshift is highly irrelevant for the impact of a cD on strong cluster lensing, we only take the simulation snapshots at redshift $z_L=0.275$, where the number of simulated arcs is largest and thus the uncertainties in the numerically determined cross sections are smallest.

3.2. Lensing simulations

The lensing properties of the numerical clusters are studied using the ray-tracing technique. Our method has been fully described in several earlier publications (see Meneghetti et al. 2000, 2001). We thus give only a brief description here, referring the reader to those papers for further detail.

Each numerical cluster is centred within a cube of $3\,h^{-1}$Mpc side length. Within this box, we compute the three-dimensional density field ρ by interpolating the mass density on a regular grid of 256^3 cells, using the *Triangular Shape Cloud* method (TSC; see Hockney & Eastwood 1988). Finally, we project ρ along the three independent box sides, obtaining three surface density maps for each cluster. These are used as lens planes. Adopting this *thin screen* approximation is justified because the distances between the sources and the lens and between the lens and the observer are much larger than the physical sizes of the galaxy clusters.

We then propagate a bundle of 2048×2048 light rays through the central quarter of each of these maps. We focus on the central parts of the clusters because our analysis concerns their strong-lensing properties only. Thus, our ray-tracing simulations resolve scales of order $\sim0.2''$, at the lens redshift. The deflection angles of each ray are computed by directly summing the contributions from each mass element of the cluster.

Once the deflection angles are known, we reconstruct the images of a large number of extended background sources. They are all placed on the same plane, located at the redshift $z_s=1$. Although real sources are distributed in redshift, putting them at a single redshift is justified for the present purposes because the lens convergence changes very little with source redshift if the lens redshift is substantially smaller, as is the case here.

The sources have elliptical shape, with axial ratios randomly drawn from the range $[0.5,1]$, and their area is equal to that of a circle of $1''$ diameter. We initially distribute them on a coarse regular grid in the source plane. Then, their spatial density is iteratively increased towards the caustic curves, where the lensing effects strengthen. This increases the probability of producing long arcs and thus the numerical efficiency of the method. In order to compensate for this artificial source-density increase, we assign in the following statistical analysis to each image a statistical weight proportional to the area of the grid cell on which the source was placed.

Image reconstruction and classification is done following the technique introduced by Bartelmann & Weiss (1994) and used in Meneghetti et al. (2000, 2001, 2003). For each image, we measure its length and width. This results in a catalogue of simulated images which is subsequently analysed statistically.

3.3. Inclusion of the cD galaxy

Being linear function of mass, the total deflection angle of a ray passing through a mass distribution is the sum of the contributions from each mass element of the deflector. Therefore, in the case of a galaxy cluster, we can decompose the cluster lens into its smoothed dark matter component, plus the granular component contributed by its galaxy population (see also Meneghetti et al. 2000). For both the cluster and the galaxies, the main

constituent is given by the dark matter which forms their halos. Our model of the cluster containing a cD galaxy can thus be fairly simple; we take the smoothed dark matter distribution obtained from the numerical simulations described above, and introduce a dark-matter halo resembling the galaxy. For each ray traced through the lens plane, we compute the deflection angle by summing the contributions from the cluster itself and the galaxy haloes.

Using this approach, the reduced deflection angle of each ray parameterised by its cell numbers (i, j) on the grid in the image plane is given by

$$\vec{\alpha}_{ij} = \vec{\alpha}_{ij}^{\rm cl} + \vec{\alpha}_{ij}^{\rm cD} \, , \tag{13}$$

where $\vec{\alpha}_{ij}^{\rm cl}$ and $\vec{\alpha}_{ij}^{\rm cD}$ are contributions to the deflection angle from the original cluster and the cD galaxy, respectively.

The values of $\vec{\alpha}_{ij}^{\rm cD}$ depend on the model for the cD galaxy. We first apply two axially symmetric models, namely spheres with the NFW or the singular isothermal density profile. Second, we also apply the pseudo-elliptical NFW lens model (Meneghetti et al. 2003) in order to account for the possible elongation of the matter distribution of the cD galaxy.

cD galaxies typically appear to be of elliptical shape, with isophotal axis ratios $b/a \sim 0.8$ (Porter et al. 1991). Moreover, the orientation of the brightest cluster ellipticals is usually not random, but correlates well with that of their host cluster (Sastry 1968; Rood & Sastry 1972; Austin & Peach 1974; Carter 1980; Binggeli 1982; Struble & Peebles 1985; Rhee & Katgert 1987; Lambas et al. 1988; Garijo et al. 1997). Asymmetries in the lensing matter distribution are known to improve the ability of the cluster to produce long and thin arcs. We also expect that the impact of a cD galaxy described by an elliptical model is largest when its orientation is aligned with the elongation direction of the host galaxy cluster. In the case of different orientations, the cD galaxy tends to circularise the mass distribution of the cluster in its central region. In order to quantify this effect, we carry out two sets of simulations; in the first, we randomly choose the orientation of the cD galaxy inside the cluster, while in the second the orientation is chosen such that the directions of the major and minor axes of the galaxy align with the major and minor eigenvalues of the cluster's deflection angle field, respectively. The galaxy ellipticity is assumed to be $e = 0.2$ (Porter et al. 1991).

The position of the cD galaxy is chosen to coincide with the minimum of the deflection angle field of the numerical galaxy cluster. This choice intentionally maximises the contribution of the cD galaxy to the total deflection angles.

4. RESULTS

4.1. *Convergence maps and critical curves*

We describe in this Section how the cD galaxy changes the projected mass distribution of the numerical clusters. The surface density map of a lens can be reconstructed from the deflection angles once the effect of the cD galaxy has been included. Indeed, the scaled surface density κ (or convergence) at each position $\vec{x}$ on the lens plane is given by

$$\kappa(\vec{x}) = \frac{\Sigma(\vec{x})}{\Sigma_{\rm cr}} = \frac{1}{2}\vec{\nabla} \cdot \vec{\alpha}(\vec{x}) \, . \tag{14}$$

Some examples for convergence maps are shown in Fig. (3). The original convergence map of the cluster, i.e. before adding the cD galaxy, is plotted in the top left panel. Then, starting from the top central panel, we show the convergence maps for all cD galaxy models we use, followed by the convergence map of the cluster including the cD galaxy: the NFW sphere (top central and top right panels), SIS (middle left and middle central panels), the pseudo-elliptical NFW model both randomly oriented (middle right and bottom left panels) and aligned with the orientation of the cluster mass distribution (bottom central and bottom left panels). The virial mass of the cD galaxy is the largest we have tested in our simulations ($5 \times 10^{13} h^{-1} M_{\odot}$). The angular scale of each plot is approximately $\sim 50''$.

The contours of the convergence maps show that the presence of the cD galaxy affects the matter distribution of the cluster only in its very central part. The size of the region where the convergence enhancement is significant depends on the model which is used to describe the cD galaxy. For example, the SIS has a steeper density profile at the centre and thus its contribution to the host cluster's surface density is significant only in a very limited region. On the other hand, due to its shallower density profile, the mass of a cD galaxy modelled as an NFW sphere or as a pseudo-elliptical NFW model is distributed across a larger region around the cluster centre. Moreover, when the pseudo-elliptical model is used, convergence contours appear to be more extended and particularly elongated if the cD galaxy is aligned with the orientation of the underlying cluster mass distribution.

Arcs form along the critical curves, where the determinant of the Jacobian matrix $A(\vec{x}) = \partial\vec{y}/\partial\vec{x}$ vanishes. Given that the dimension-less coordinates on the source plane $\vec{y}$ and on the lens plane $\vec{x}$ are related by the lens equation, $\vec{y} = \vec{x} - \vec{\alpha}(\vec{x})$, the position of the critical curves can be easily found through numerical derivatives of the deflection angles. Then, using the lens equation, we can find the position of the caustics, near which sources must be located in order to be strongly magnified.

We show in Fig. (4) some examples of critical curves and caustics for the most massive (first two rows of panels) and the least massive (last two rows of panels) clusters in our sample (in the ΛCDM model). In each panel, we plot the results before adding the cD galaxy (thick curves), and after including the contribution to the deflection angles from a cD galaxy with a virial mass of $5 \times 10^{13} h^{-1} M_{\odot}$ (thin curves). In the first column on the left, we show the results obtained by modelling the cD as an NFW sphere; in the second column, we plot the critical curves and caustics found modelling the galaxy as pseudo-elliptical, randomly oriented NFW models; in the third column, we show the results for the pseudo-elliptical NFW model aligned with the orientation of the underlying cluster matter distribution; and in the fourth column we finally show the critical curves and the caustics obtained modelling the cD as a SIS.

As expected, the critical curves and the caustics appear to be pushed towards larger cluster-centric radii when the cD galaxy is included into the simulations. The largest effect is produced by the pseudo-elliptical cD if its orientation is aligned with that of the host cluster. The singular isothermal cD has the least effect on the critical curves. Of course, the impact of the cD galaxy is different on clusters with different masses. For example, the caustics of the most massive lens demonstrate that they are affected by the presence of the cD only far from the cusps. This is not the case for the least massive cluster, where also the cusp positions are pushed away from the lens centre. Also, the critical curves appear to be more extended once the cD is added to the least massive cluster. Of course, this is due to the fact that, by adding the cD, we are changing the cluster mass in its central region by a different percentage. Similar results are found for clusters in the OCDM model.

4.2. *Tangential arcs*

Tangential arcs are selected from the catalogues of simulated images for each numerical cluster model by requiring a minimal length-to-width ratio. We then quantify the cluster's efficiency

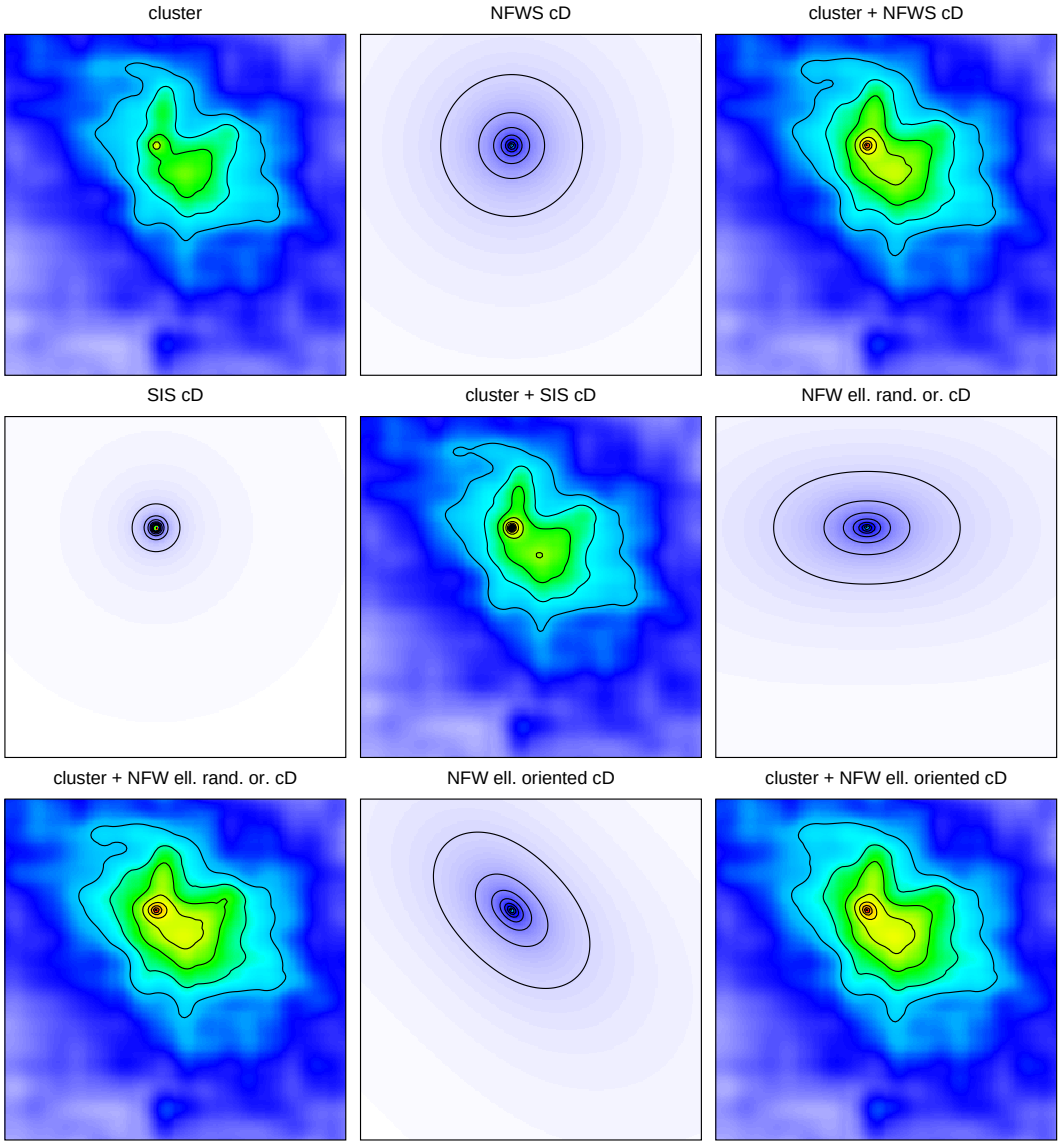

FIG. 3.—Examples of convergence maps for one of the clusters in the GIF sample and for the cD galaxy models. Starting from the top-left panel: (a) cluster without the cD galaxy; (b) cD galaxy of mass $M_{\rm cD} = 5 \times 10^{13}\, h^{-1}\, M_{\odot}$ with NFW density profile; (c) cluster with the cD galaxy modelled as in (b); (d) cD galaxy with the same mass, but with SIS density profile; (e) cluster with the cD galaxy modelled as in (d); (f) pseudo-elliptical NFW model randomly oriented with respect to the cluster mass distribution; (g) cluster with the cD galaxy modelled as in (f); (h) pseudo-elliptical NFW model with its orientation aligned with that of the cluster mass distribution; (i) cluster with the cD galaxy modelled as in (h).

for producing this type of arcs by measuring its lensing cross section. This procedure is carried out for all numerical clusters before and after the inclusion of the cD galaxy.

By definition, the lensing cross section is the area on the source plane where a source must be located in order to be imaged as an arc with the specified property. As explained in Sect. 3.2., each source is taken to represent a fraction of the source plane. We assign a statistical weight of unity to the sources which are placed on the sub-grid with the highest resolution. These cells have area A. The lensing cross section is then measured by counting the statistical weights of the sources whose images satisfy a specified property. If a source has multiple images with the required characteristics, its statistical weight is multiplied by the number of such images. Thus, the formula for computing cross sections for arcs with a property p is

$$\sigma_{\rm p} = A \sum_i w_i\, n_i \ , \qquad (15)$$

where n_i is the number of images of the i-th source satisfying the required conditions, and w_i is the statistical weight of the source.

We compute the lensing cross sections for arcs whose length-to-width ratio (L/W) exceeds a lower threshold $(L/W)_{\rm min}$. The results obtained for each cluster with and without the cD galaxy are compared by computing the relative change of the cross sections due to the presence of the cD.

We show in Figs. (5) and (6) the relative change of the lensing cross sections for long and thin arcs as a function of the cluster virial mass for the simulations in the ΛCDM and in the OCDM models. The panels in the left, central and right columns show the relative change of the cross sections for arcs with length-to-width ratios $(L/W) > 5$, $(L/W) > 7.5$ and $(L/W) > 10$, respectively. In each panel, we plot the results for all four models used to describe the cD galaxy. The top, middle and bottom panels refer to simulations in which the virial mass of the cD galaxy is $(5 \times 10^{12}, 10^{13}, 5 \times 10^{13})\, h^{-1}\, M_{\odot}$, respectively.

As expected, the largest variations of the cross sections are

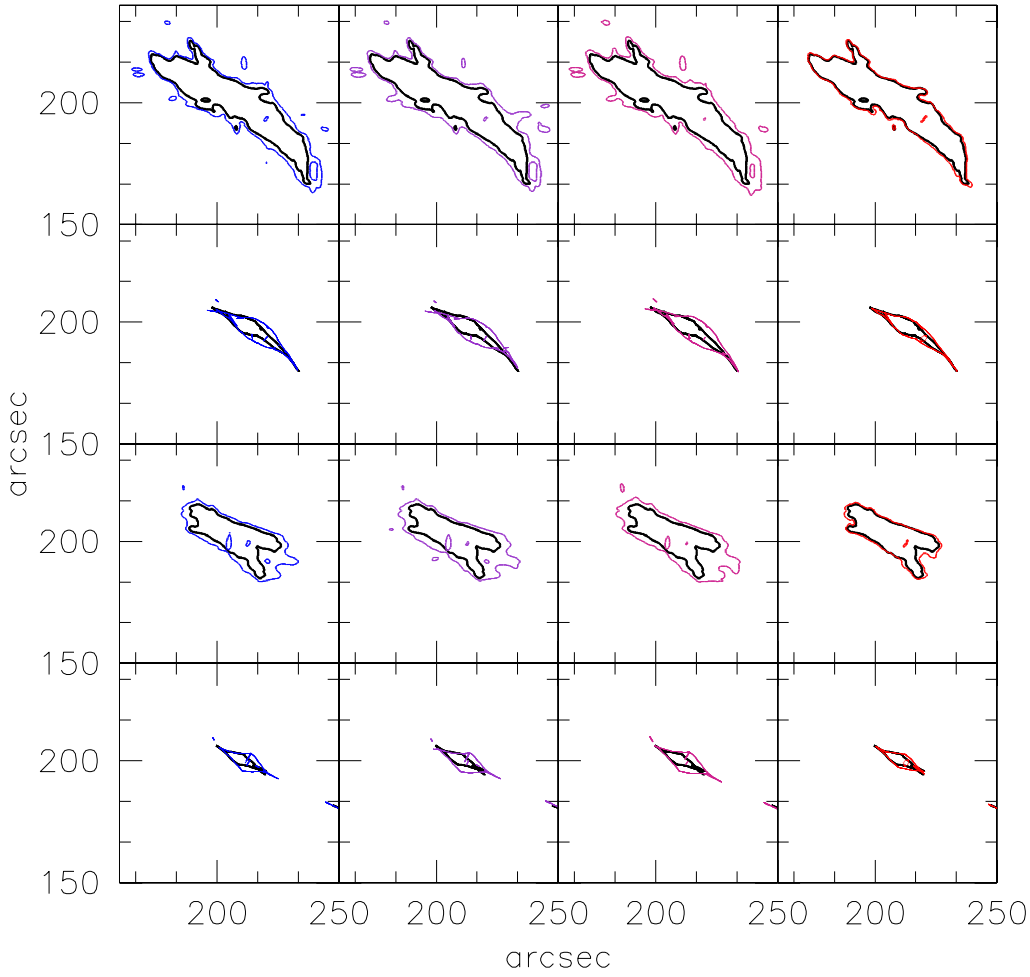

FIG. 4.—Examples of critical curves and caustics. The first row of panels shows how the critical curves for one projection of the most massive cluster ($M \sim 10^{15}\,h^{-1}\,M_{\odot}$) in the GIF sample change in response to the inclusion of the cD galaxy. In each panel, we draw the original critical curves (bold curves) and those modified by the cD (thin curves). We show the results obtained by modelling the cD galaxy as an NFW sphere (first column from the left); using the pseudo-elliptical model randomly oriented (second column) and aligned with the cluster mass distribution (third column), and as a SIS (fourth column). The panels in the second row show the corresponding caustic curves. Similarly, we plot in the third and in the fourth row of panels the critical curves and the caustics for one projection of the least massive cluster in the sample ($M \sim 3 \times 10^{14}\,h^{-1}\,M_{\odot}$). The mass of the cD galaxy is $M_{\rm cD} = 5 \times 10^{13}\,h^{-1}\,M_{\odot}$, and the background cosmology is the ΛCDM model.

typically found if the cD galaxy is modelled as a pseudo-elliptical NFW model whose orientation is aligned with that the host cluster. On the other hand, cD galaxies with SIS profiles change the ability of the numerical clusters for producing long and thin arcs only by a very small amount.

In the ΛCDM model, a cD galaxy with mass between $M_{\rm cD} = 5 \times 10^{12}\,h^{-1}\,M_{\odot}$ and $M_{\rm cD} = 10^{13}\,h^{-1}\,M_{\odot}$ produces maximal variations on the order of $40\% - 50\%$. More massive cDs have a stronger impact on the strong-lensing efficiency of the clusters: a galaxy with mass $M_{\rm cD} = 5 \times 10^{13}\,h^{-1}\,M_{\odot}$ changes the lensing cross section by a maximum amount between 60% and 200%, depending on the total cluster mass. The impact of the cD is generally larger in the less massive clusters.

A similar trend is found in the OCDM model, but the variations of the cross sections are smaller in this case. For example, in the simulations with the most massive cDs, the cross sections change by approximately $40\% - 80\%$ only. This behaviour was expected because the clusters in the OCDM model are generally more compact compared than those in the ΛCDM model. Including the cD, the mass in the very central part of the clusters changes less compared to the clusters in the ΛCDM model. Cross sections for arcs with different minimal length-to-width ratios show similar variations.

4.3. *Radial arcs*

The appearance and location of radial arcs within the lensing clusters is determined by several factors, among them the slope of the projected density profile and the central density of the lens. The steeper the density profile is, the closer to the centre the radial arcs move. Moreover, the higher the central surface density is, the larger is the extent of the radial critical line.

Radial arcs are quite rare events. Many clusters in our sample exhibit very short radial critical curves and are thus not very efficient in producing radially distorted images. In particular, the numerical clusters in our sample have significantly smaller cross sections for radial arcs in the ΛCDM than in the OCDM model. The reason is that the clusters in the ΛCDM model are less con-

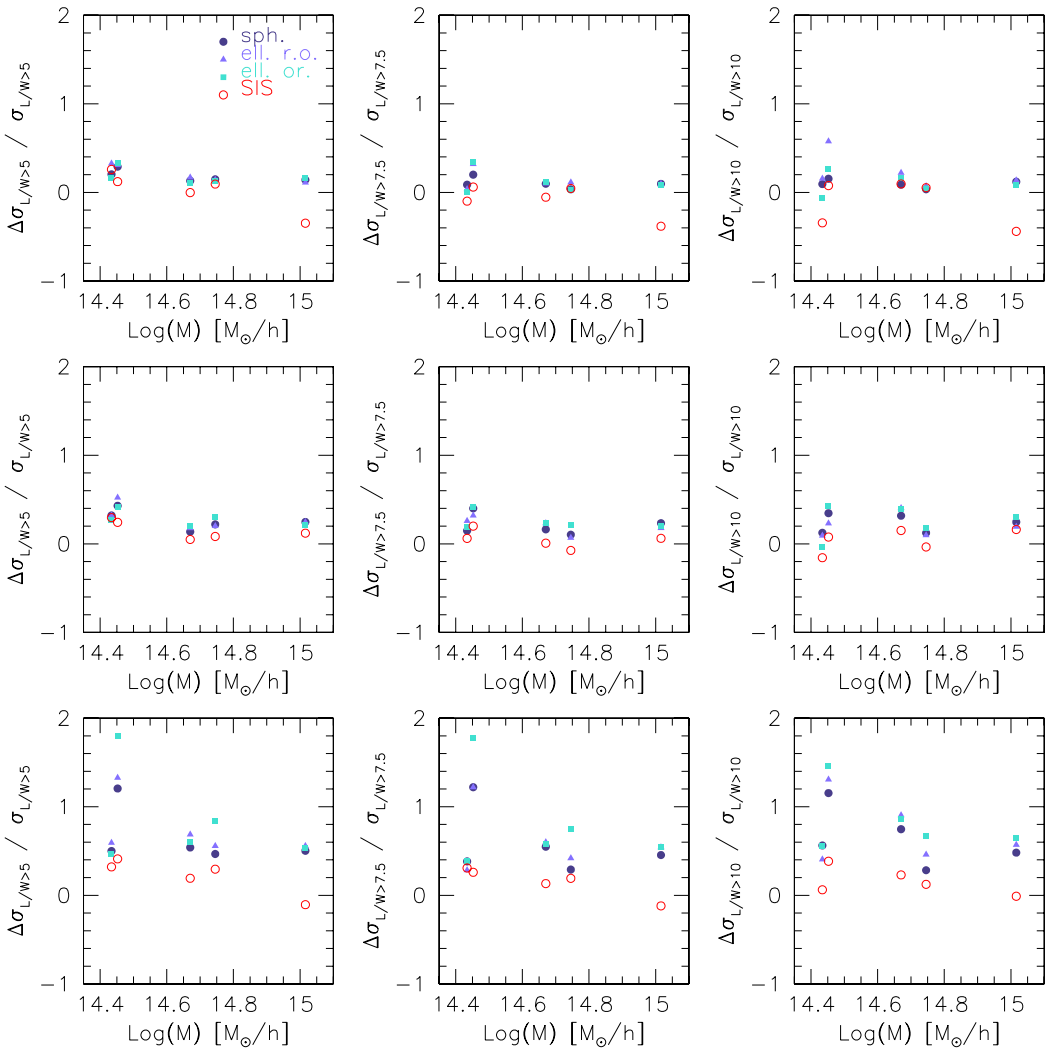

FIG. 5.—Relative change in the cross sections for arcs with length-to-width ratios exceeding 5 (left column), 7.5 (central column) and 10 (right column) as a function of cluster mass for the numerically simulated clusters in the ΛCDM model. Results are shown for three different masses of the cD galaxy: $5\times10^{12}\,h^{-1}\,M_\odot$ (top panels), $10^{13}\,h^{-1}\,M_\odot$ (middle panels) and $5\times10^{13}\,h^{-1}\,M_\odot$ (bottom panels). Filled circles, triangles and squares mark the results obtained modelling the cD as an NFW sphere, a pseudo-elliptical NFW model with random orientation, and aligned with the orientation of the host cluster, respectively; open circles show the results found modelling the cD galaxy as a SIS.

centrated than in the OCDM model. Given that we increase the mass in the inner part of the numerical clusters by quite a large amount by adding a massive cD galaxy, we expect that the capability of the cluster models for producing radial arcs should be increased when a cD galaxy is included. For investigating this question, we again compare the lensing cross sections for radial arcs of the numerical models before and after including a cD galaxy.

Radial arcs are identified from the complete sample of distorted images using the technique described by Meneghetti et al. (2001). It consists in selecting those arcs for which the measured radial magnification at their position exceeds a lower threshold. The relative change of the lensing cross section for this type of arcs as a function of the original lensing cross section of clusters not containing a cD galaxy is shown in Fig. (7). The cD galaxy mass is $5\times10^{13}\,h^{-1}\,M_\odot$. In the left and right panels, we plot the results for the cluster models in the ΛCDM and in the OCDM models, respectively. Again we use circles, squares and triangles for identifying different cD galaxy models, using the same symbols as in Figs. (5) and (6).

As the figure shows, the cD galaxy increases the capability of the cluster models for producing radial arcs, but this enhancement depends on the original size of their lensing cross sections. Clusters which were less efficient in producing radial arcs increase their lensing cross sections by roughly 500%, while this increment is smaller for lenses which already produced a higher number of radial arcs. In particular, the effect of the cD galaxy on the lensing cross sections of clusters is significantly larger in the ΛCDM model compared to the OCDM model. One of the clusters in our sample (the least massive one) did not produce any radial arcs before a cD galaxy was included, thus the results for only four clusters are shown in Fig. (7).

5. SUMMARY AND CONCLUSIONS

We investigated the effect of massive cD galaxies on the strong-lensing properties of galaxy clusters. The main motivation behind our study is to identify possible reasons for the pronounced failure of numerical cluster-lensing models in the strongly favoured ΛCDM cosmology in reproducing the observed abundance of giant luminous arcs.

Although inadequate for quantitatively reliable results, our

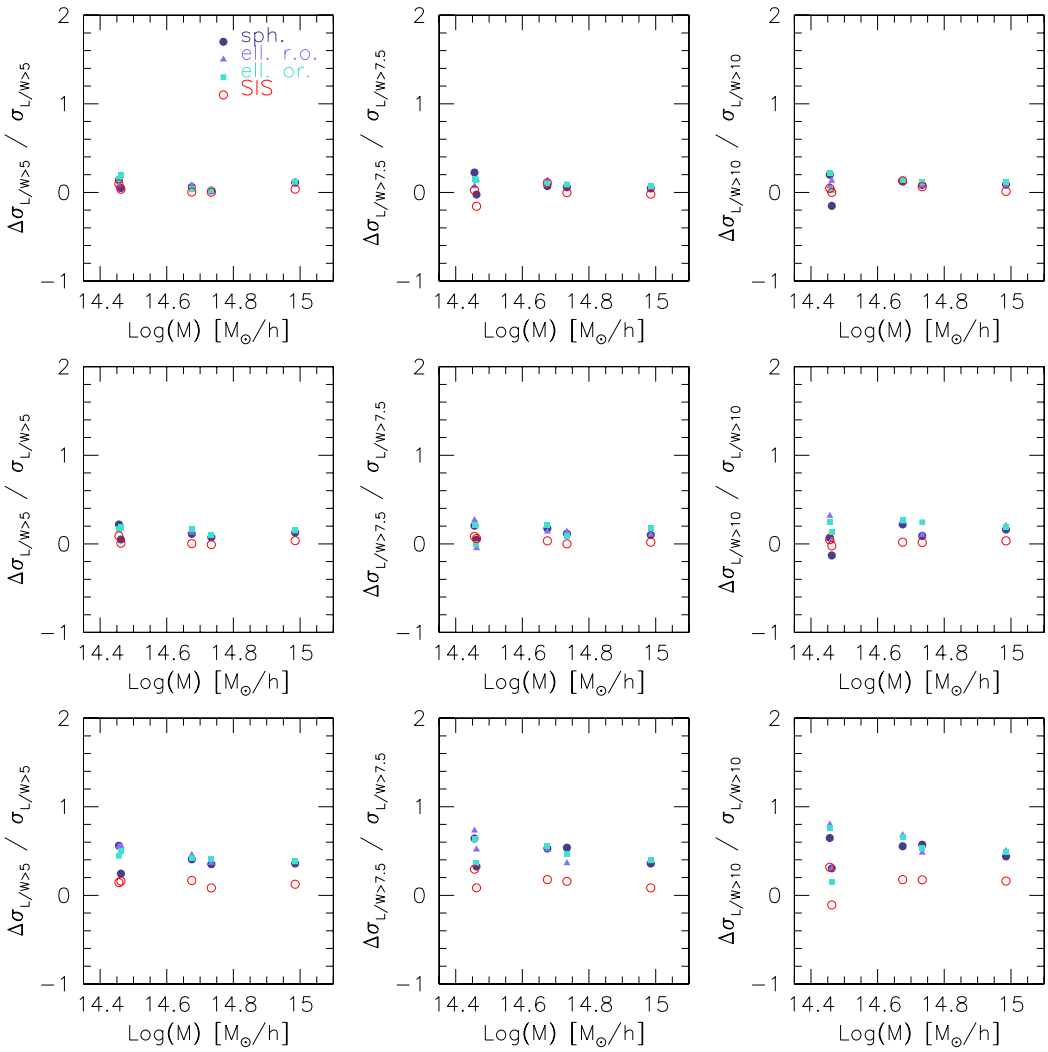

FIG. 6.—Relative change in the cross sections for arcs with length-to-width ratios exceeding 5 (left column), 7.5 (central column) and 10 (right column) as a function of cluster mass for the numerically simulated clusters in the OCDM model. Results are shown for three different masses of the cD galaxy: $5\times10^{12}\,h^{-1}\,M_\odot$ (top panels), $10^{13}\,h^{-1}\,M_\odot$ (middle panels) and $5\times10^{13}\,h^{-1}\,M_\odot$ (bottom panels). Circles, squares and triangles identify different cD galaxy models with the same symbols as in Fig. (5).

analytic model demonstrated three interesting aspects of the problem. First, the effect of cD galaxies is much stronger in clusters with NFW rather than singular isothermal density profile because of the flatter central density profile of the former. Second, cD galaxies are expected to be much less efficient in asymmetric than in axially symmetric clusters because the stronger gravitational tidal field in asymmetric clusters makes the relative contribution of the additional central mass component less important. Third, the impact of cD galaxies on the strong-lensing properties of clusters is expected to be almost independent of lens redshift.

We then carried out ray-tracing simulations using massive numerically simulated galaxy clusters in the ΛCDM and OCDM cosmologies to which we added cD galaxies in four different ways; either modelled as singular isothermal spheres or modelled with the NFW density profile, either axially symmetric or elliptically distorted; and if distorted, either oriented randomly or aligned with the orientation of the cluster mass distribution. All cD galaxies are placed at the minima of the deflection-angle maps of the cluster models. They have masses of 5×10^{12}, 10^{13}, or $5\times10^{13}\,h^{-1}\,M_\odot$, which are added to the cluster mass.

Note that these choices yield conservative results because they tend to exaggerate the possible effects. The cD-galaxy masses are *very* high, in particular compared to the least massive cluster of our sample, and they are *added* to the clusters without correspondingly decreasing the cluster mass.

Although we find relative enhancements of large-arc cross sections by up to $\sim 200\%$ for our least massive cluster if a cD galaxy with $5\times10^{13}\,h^{-1}\,M_\odot$ and an elliptically distorted NFW density profile is added with its orientation aligned with the mass distribution of the cluster, such a situation can hardly be considered realistic because that cD galaxy has $\sim 20\%$ of the cluster mass. In more realistic cases of cD galaxies with $\lesssim 10^{13}\,h^{-1}\,M_\odot$, tangential-arc cross sections are increased by not more than $\sim 50\%$. It should be noted, however, that we have to compare the relative increase between clusters in ΛCDM and OCDM models, which is typically not more than $\sim 30\%$.

Cross sections for the formation of radial arcs are much more affected because they are highly sensitive to the exact central density profile of the cluster lenses. The presence of a cD galaxy can multiply the radial-arc cross sections by factors of a few, typically up to five in the ΛCDM model. This reinforces the finding by other authors that radial-arc statistics potentially is a highly significant tracer for central density profiles of clusters, but as

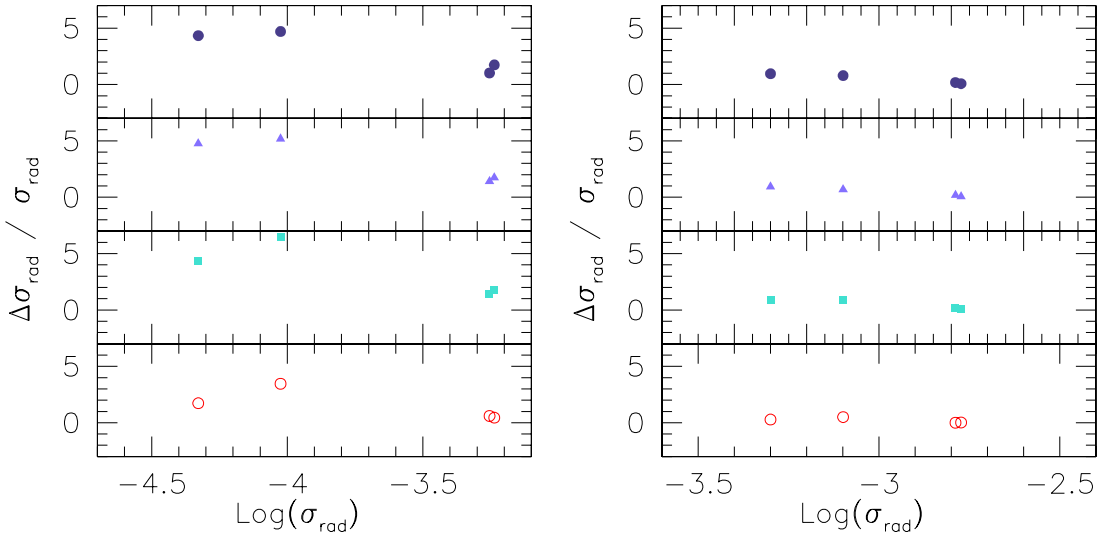

FIG. 7.—Relative change of the cross section for radial arcs versus original cross sections (i.e. before the inclusion of a cD galaxy). The left and right panels show the results obtained in the ΛCDM and the OCDM models, respectively. We use circles, squares and triangles to identify different cD galaxy models, using the same symbols as in Figs. (5) and (6).

such less suitable for constraints on cosmological parameters. Currently, also, the data base for radial arc statistics is rather too poor for any meaningful conclusions.

We thus conclude from our conservative estimates of the impact of cD galaxies on strong-lensing cross sections by galaxy clusters that they may increase the arc-formation probability by perhaps up to $\sim 50\%$ in realistic situations, but certainly by far not enough for explaining the discrepancy between simulations in ΛCDM models and the observed abundance of arcs.

ACKNOWLEDGEMENTS

This work has been partially supported by Italian MIUR (Grant 2001, prot. 2001028932, "Clusters and groups of galaxies: the interplay of dark and baryonic matter"), CNR and ASI. MM thanks the EARA for financial support and the Max-Planck-Institut für Astrophysik for the hospitality during the visits when part of this work was done. We are grateful to Bepi Tormen for clarifying discussions.

REFERENCES

Austin T. B., Peach J. V., 1974, MNRAS, 168, 591
Bartelmann M., 1996, A&A, 313, 697
Bartelmann M., Huss A., Colberg J. M., Jenkins A., Pearce F. R., 1998, A&A, 330, 1
Bartelmann M., Meneghetti M., Perrotta F., Baccigalupi C., Moscardini L., 2003, preprint, astro-ph/0210066
Bartelmann M., Weiss A., 1994, A&A, 298, 1
Binggeli B., 1982, A&A, 107, 338
Bond J.R., Efstathiou G., 1984, ApJ, 285, L45
Bullock J. S., Kolatt T. S., Sigad Y., Somerville R. S., Kravtsov A. V., Klypin A. A., Primack J. R., Dekel A., 2001, MNRAS, 321, 559
Carter D., 1980, MNRAS, 190, 307
Cooray A. R., Quashnock J. M., Miller M. C., 1999, ApJ, 511, 562
de Bernardis P., Ade P. A. R., Bock J. J., et al., 2002, ApJ, 564, 559
Eke V. R., Navarro J. F., Steinmetz M., 2001, ApJ, 554, 114
Garijo A., Athanassoula E., Garcia-Gomez C., 1997, A&A, 327, 930
Gioia I. M., Luppino G. A., 1994, ApJS, 94, 583
Hockney R.W., Eastwood J.W., 1988, Computer simulations using particles. Hilger, Bristol
Kauffmann G.A.M., Colberg J.M., Diaferio A., White S.D.M., 1999, MNRAS, 303, 188
Kaufmann R., Straumann N., 2000, Ann. Phys., 11, 507
Lambas D. G., Groth E. J., Peebles P. J. E., 1988, AJ, 95, 975
Le Fevre O., Hammer F., Angonin M. C., Gioia I. M., Luppino G. A., 1994, ApJ, 422, L5
Meneghetti M., Bartelmann M., Moscardini L., 2003, MNRAS in press, astro-ph/0201501
Meneghetti M., Bolzonella M., Bartelmann M., Moscardini L., Tormen G., 2000, MNRAS, 314, 338
Meneghetti M., Yoshida N., Bartelmann M., Moscardini L., Springel V., Tormen G., White S.D.M., 2001, MNRAS, 325, 435
Molikawa K., Hattori M., 2001, ApJ, 559, 544
Molikawa K., Hattori M., Kneib J.-P., Yamashita K., 1999, A&A, 351, 413
Navarro J. F., Frenk C. S., White S. D. M., 1996, ApJ, 462, 563
Navarro J.F., Frenk C.S., White S.D.M., 1997, ApJ, 490, 493
Oguri M., Taraya A., Suto Y., 2001, ApJ, 559, 572
Oguri M., Taraya A., Suto Y., Turner E.L., 2002, ApJ, 568, 488
Perlmutter S., 1998, AAS, 30, 1388
Perlmutter S., Gabi S., Goldhaber G., et al., 1997, ApJ, 483, 565
Perrotta F., Baccigalupi C., Bartelmann M., de Zotti G., Granato G.L., 2002, MNRAS, 329, 445
Porter A. C., Schneider D. P., Hoessel J. G., 1991, AJ, 101, 1561
Rhee G. F. R. N., Katgert P., 1987, A&A, 183, 217
Rood H. J., Sastry G. N., 1972, AJ, 77, 451
Sastry G. N., 1968, PASP, 80, 252
Struble M. F., Peebles P. J. E., 1985, AJ, 90, 582
Viana P.T.P., Liddle A.R., 1996, MNRAS, 281, 323
Wu X., Hammer F., 1993, MNRAS, 262, 187
Wu X.-P., Mao S., 1996, ApJ, 463, 404